

Design radiatif de céramiques poreuses à base de CeO_2 pour la production d' H_2 par thermochimie solaire



Pierre-Marie Geffroy, Thierry Chartier, Stéphane Abanades,
Benoit Rousseau



LTen UMR CNRS 6607, Nantes, France
benoit.rousseau@univ-nantes.fr 0033663287203



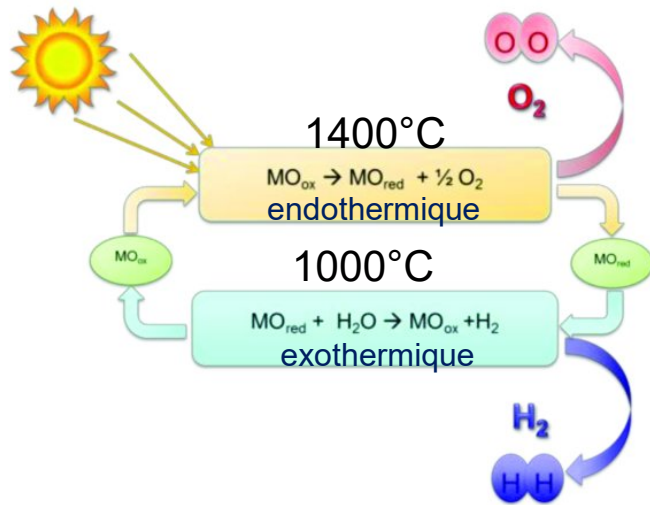
celluleenergie.cnrs.fr

Cycle thermochimique “haute température” en 2 étapes

Décomposition thermique de la vapeur d'eau



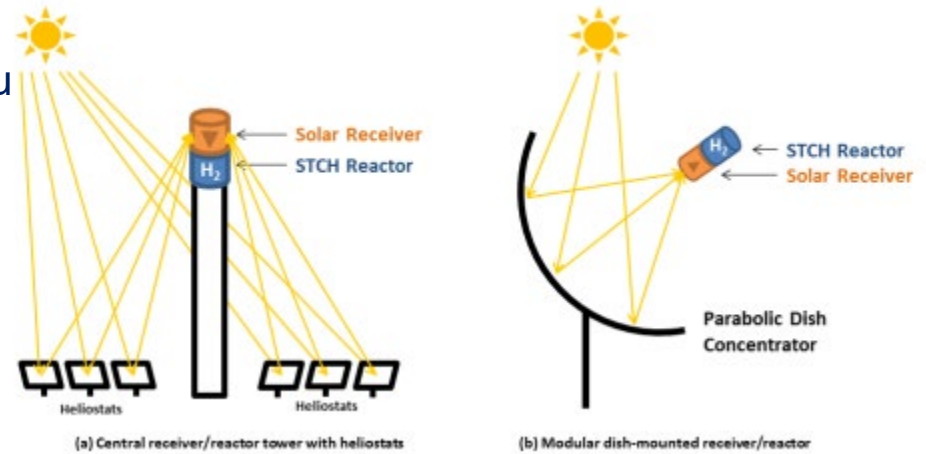
Dissociation thermochimique de la vapeur d'eau



Fort intérêt pour l'oxyde de cérium $\text{CeO}_{2-\delta}$:

- Stabilité thermique ($T > 1400^\circ\text{C}$)
- Bonne cinétique d'oxydation ($\sim 1000^\circ\text{C}$),
- Bon taux de diffusion de l'oxygène
- Bonne disponibilité d'approvisionnement

Apport de chaleur

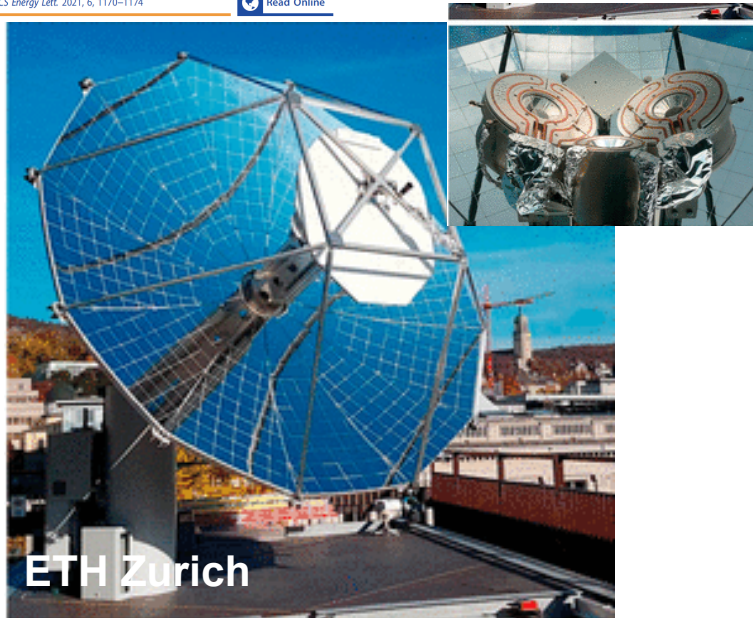


Phénomènes physiques complexes :

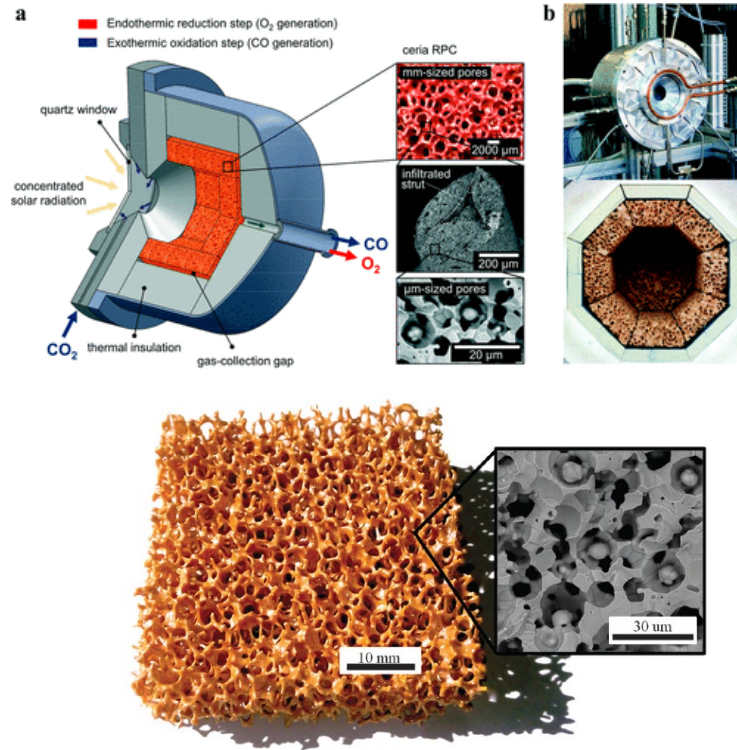
- Transferts radiatifs couplés
- Écoulement fluide gazeux (laminaire)
- Réactions chimiques
- Approches modélisations homogénéisés/discrètes

Réacteurs solaires pour la production de H₂

Technology Readiness Level of Solar Thermochemical Splitting Cycles

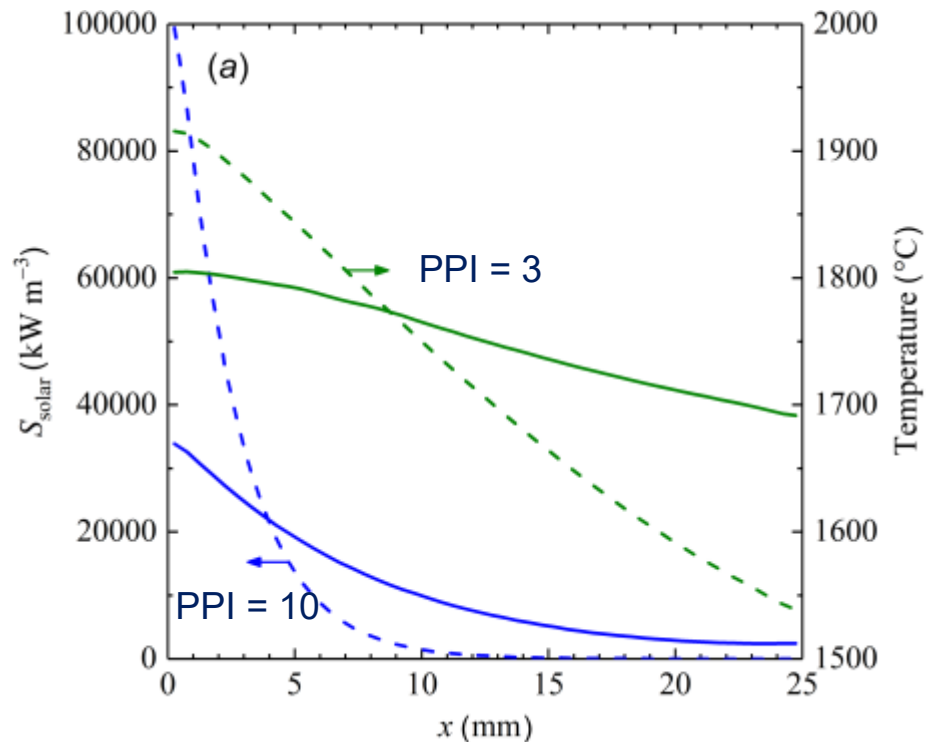


- Réacteur 4 kW / 0.002 m²
- Concentration : 3000 suns
- Efficacité de conversion solaire-H₂ ~ 5.25 %
- Mise en œuvre d'un second réacteur 50 kW, IMDEA Madrid



Limitations actuelles liées à la géométrie des mousses de CeO₂

- Efficacité de conversion solaire-H₂ ~ 20-25 % pour rentabilité économique
- Manque d'homogénéité de chauffage lors de l'étape de réduction (lié au chauffage sur une face) → chauffage volumique
- Etape d'oxydation requiert sur une surface volumique la plus élevée possible
- Identifier structure poreuse garantissant une bonne productivité d'H₂ par kg de CeO₂
- PPI = 3 → pores = 7 mm → gradient = 113°C
- PPI = 10 → pores = 2 mm → gradient = 377°C



Heat Transfer Model of a 50 kW Solar Receiver-Reactor for Thermochemical Redox Cycling Using Cerium Dioxide

This work reports on the development of a transient heat transfer model of a solar receiver-reactor designed for thermochemical redox cycling by temperature and pressure swing of pure cerium dioxide in the form of a reticulated porous ceramic (RPC). In the first, endothermic step, the cerium dioxide RPC is directly heated with concentrated solar radiation to 1500 °C while under vacuum pressure of less than 10 mbar, thereby releasing oxygen from its crystal lattice. In the subsequent, exothermic step, the reactor is repressurized with carbon dioxide as it cools, and at temperatures below 1000 °C, the partially reduced cerium dioxide is re-oxidized with a flow of carbon dioxide. To analyze the performance of the solar reactor and to gain insight into improved design and operational conditions, a transient heat transfer model of the solar reactor for a solar radiative input power of 50 kW during the reduction step was developed and implemented in ANSYS cfx. The numerical model couples the incoming concentrated solar radiation using Monte Carlo ray tracing, incorporates the reduction chemistry by assuming thermodynamic equilibrium, and accounts for internal radiation heat transfer inside the porous ceria by applying effective heat transfer properties. The model was experimentally validated using data acquired in a high-flux solar simulator (HFSS), where temperature evolution and oxygen production results from model and experiment agreed well. The numerical results indicate the prominent influence of solar radiative input power, where increasing it substantially reduces reduction time of the cerium dioxide structure. Consequently, the model predicts a solar-to-fuel energy conversion efficiency of >5% at a solar radiative power input of 50 kW; efficiency >10% can be obtained provided the RPC macroporosity is substantially increased, and better volumetric absorption and uniform heating is achieved. Managing the ceria surface temperature during reduction to avoid sublimation is a critical design consideration for direct absorption solar receiver-reactors. [DOI: 10.1115/1.4042059]

Keywords: solar energy, thermochemical cycles, ceria, reticulated porous ceramic, reactor modeling, design optimization

S. Zoller
Department of Mechanical and
Process Engineering,
ETH Zurich,
Zurich 8092, Switzerland

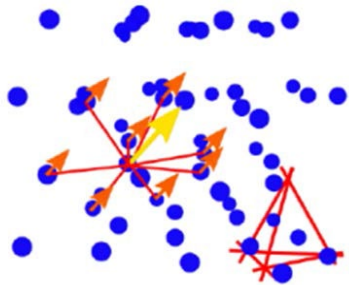
E. Koepf¹
Department of Mechanical and
Process Engineering,
ETH Zurich,
Zurich 8092, Switzerland
e-mail: koepf@ethz.ch

P. Reos
Department of Mechanical and
Process Engineering,
ETH Zurich,
Zurich 8092, Switzerland

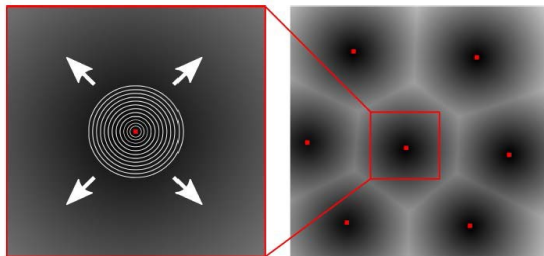
A. Steinfeld
Department of Mechanical and
Process Engineering,
ETH Zurich,
Zurich 8092, Switzerland

Génération numérique de structures poreuses (genMat, C++, Qt)

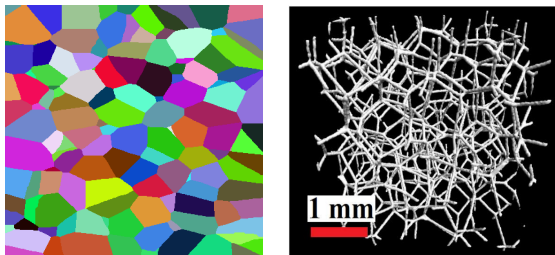
Algorithme



Ensemencement de graines

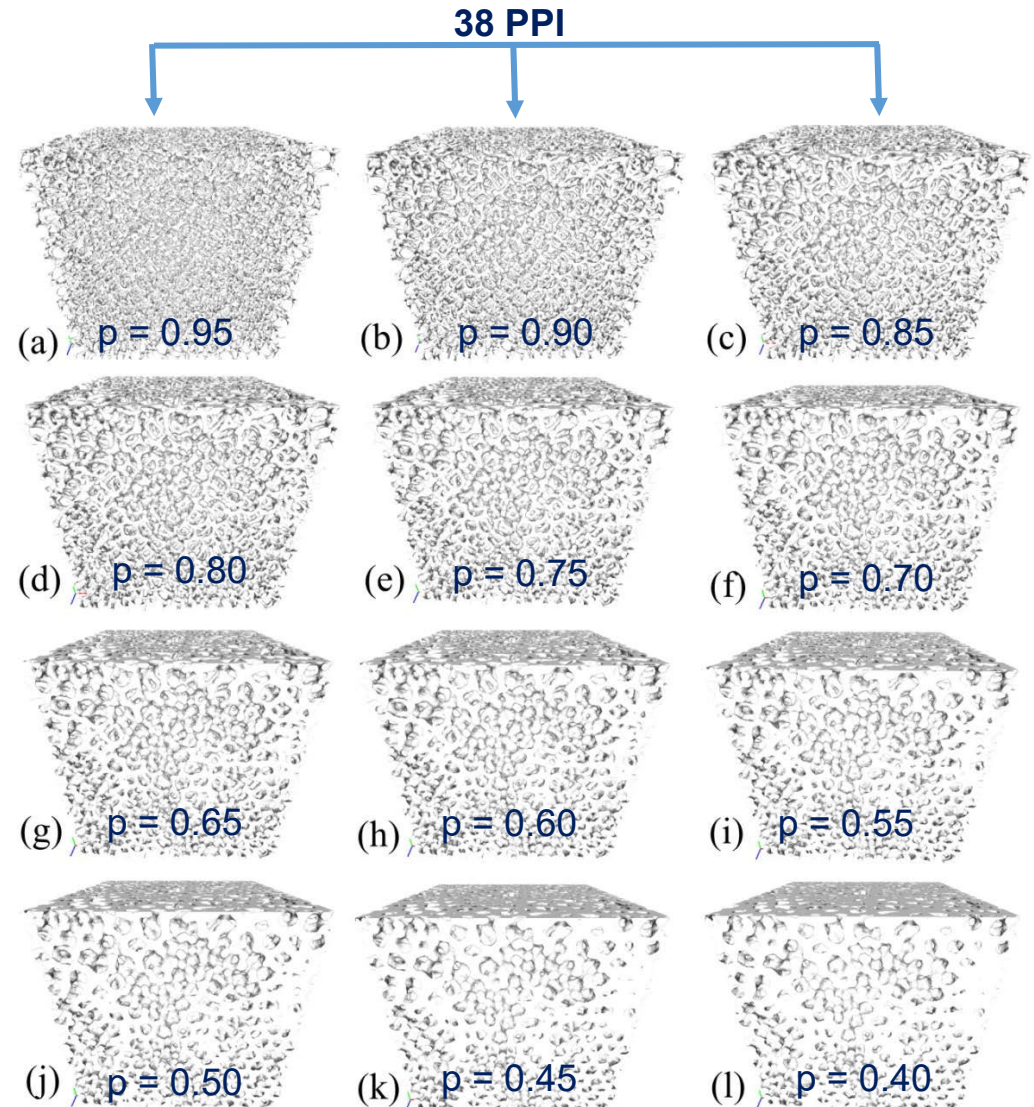


Algorithme de fast-marching



Segmentation

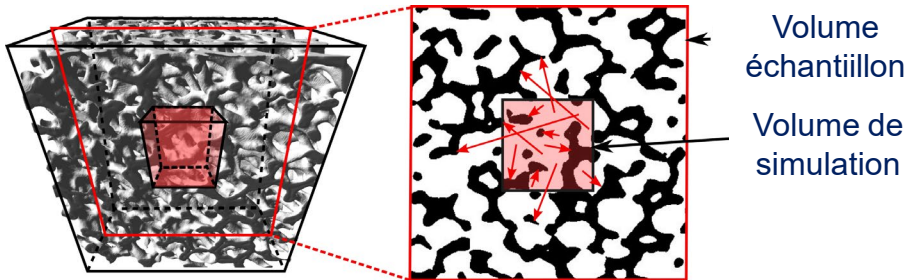
Squelettisation



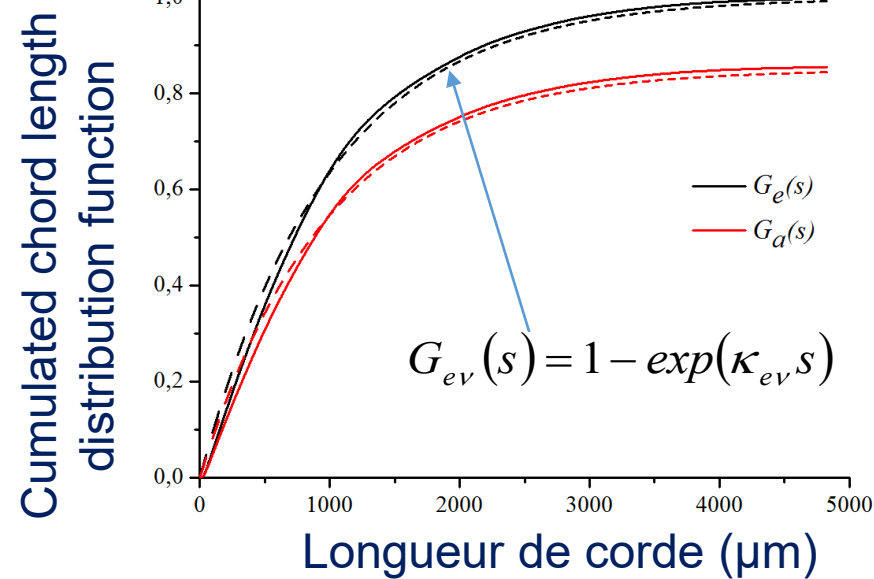
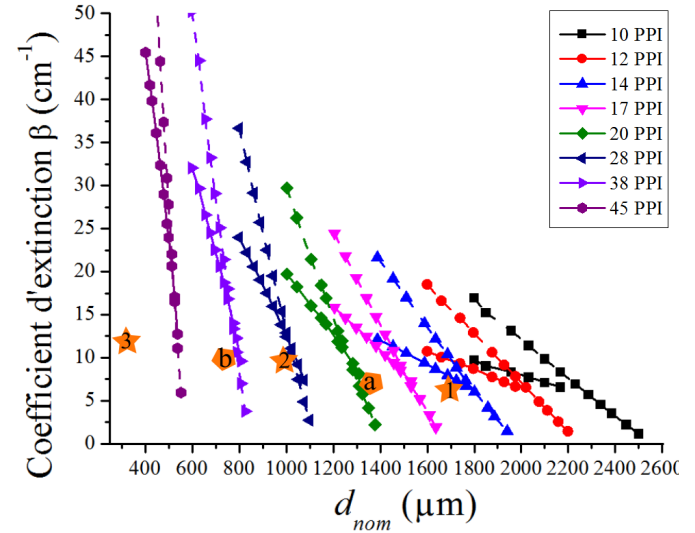
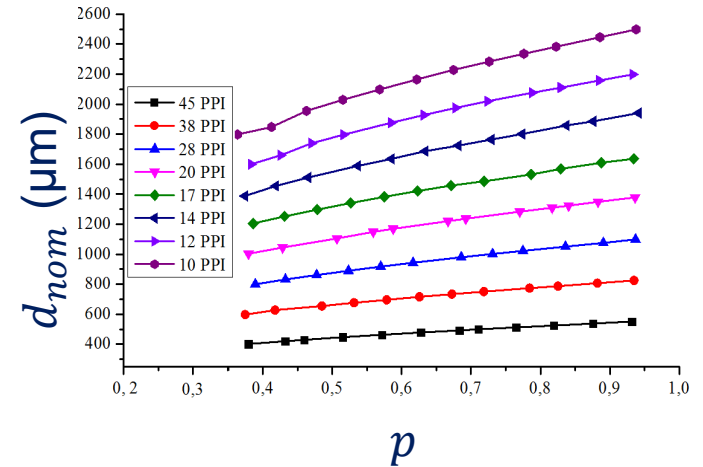
Génération numérique de structures poreuses (genMat, C++, Qt)

Méthode d'identification statistique

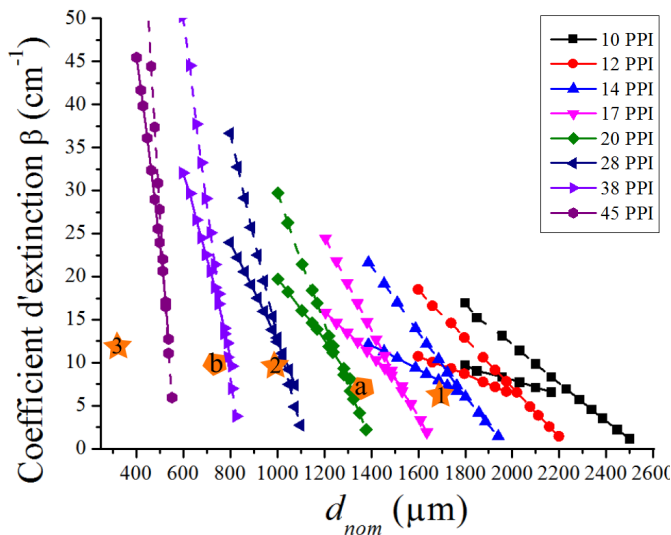
Tancrez et al., *IJHMT*, 2004, 47, 373–383



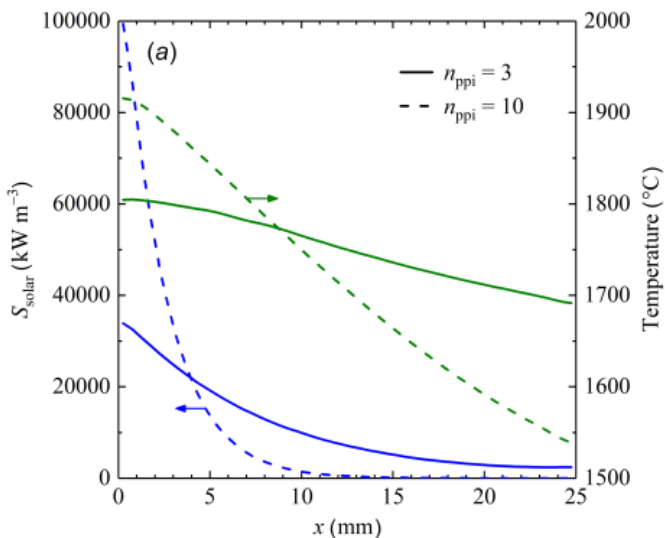
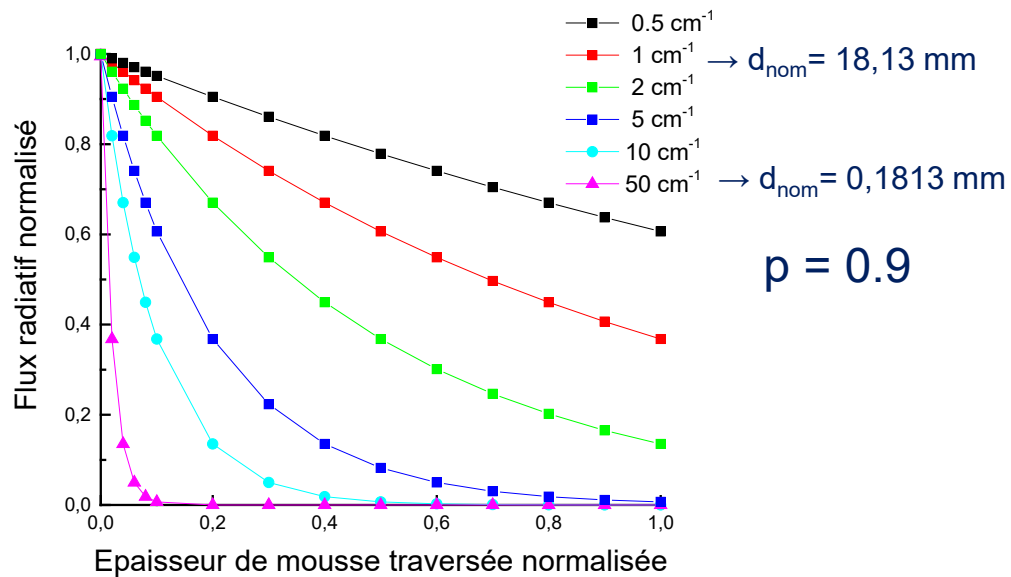
Guévelou et al., *JPM*, 2015, 18, 1031-1045



Vers la recherche de matériaux poreux à texture plus inhomogène

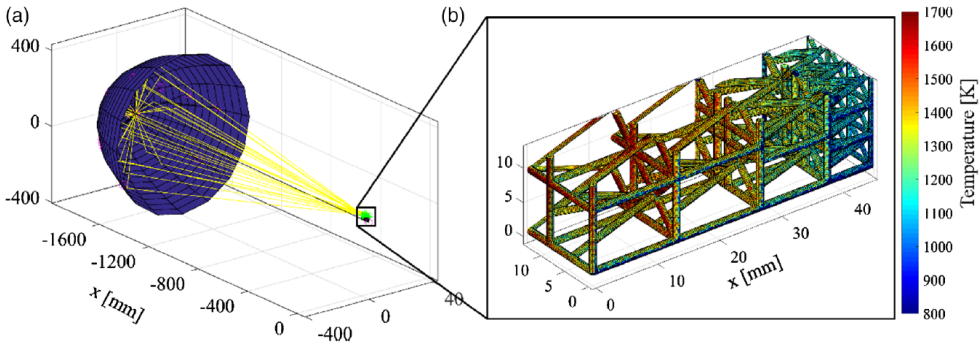
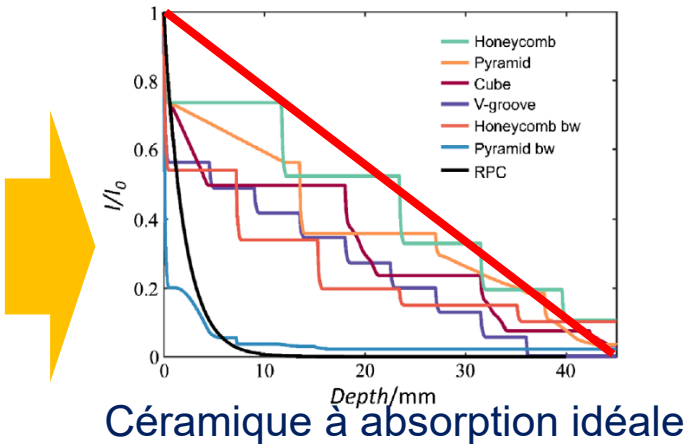
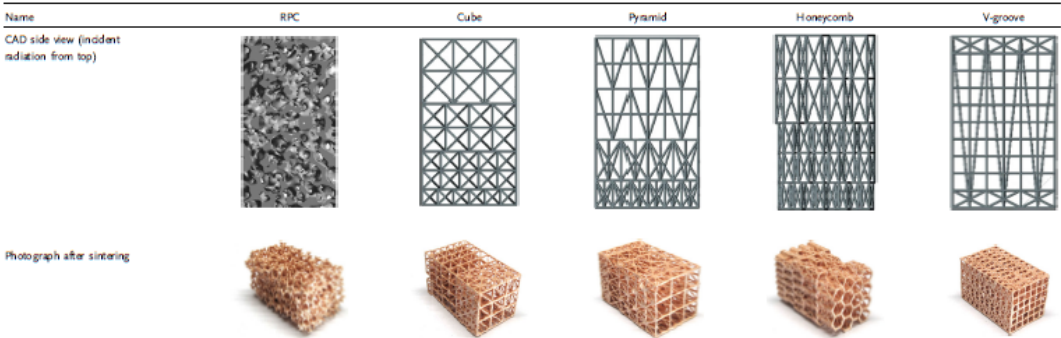


$$\kappa_{ev} = 2.45 \frac{(1 - 0.7p)}{d_{nom}}$$



petit PPI \leftrightarrow haut d_{nom} \leftrightarrow petit coefficient d'extinction

Nouvelles géométries 3D par fabrication additive

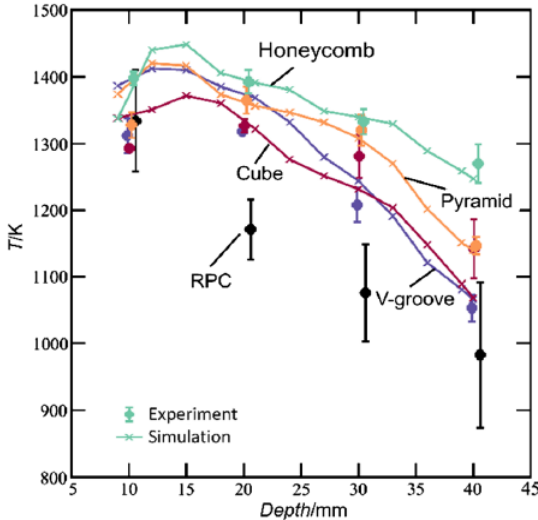


FULL PAPER



Additive-Manufactured Ordered Porous Structures Made of Ceria for Concentrating Solar Applications

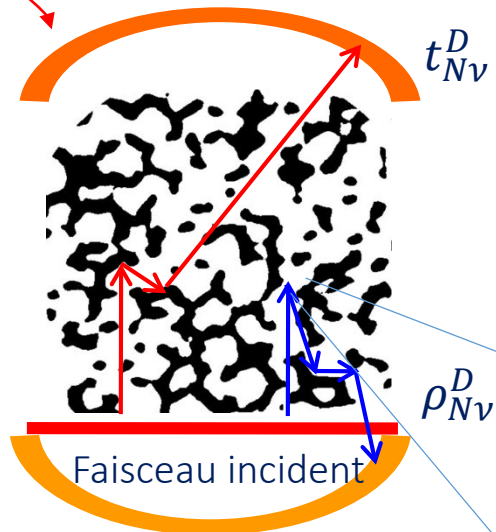
Marie Hoes, Simon Ackermann, David Theiler, Philipp Furler, and Aldo Steinfeld*



Réduction gradient thermique

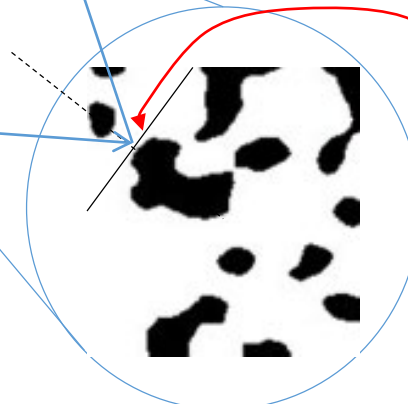
Caractérisation de la propagation volumique du rayonnement

Code de Monte Carlo Lancer de Rayon :
genMat (C++, Qt)



Echelle macroscopique: $\sim 10000 \mu\text{m}$

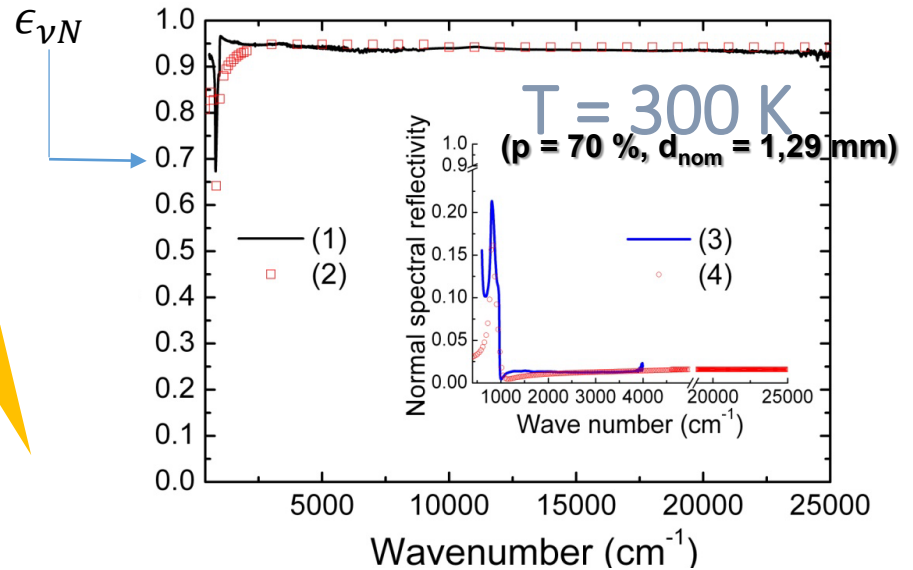
Rousseau et al., JCPS, 2012
Guevelou et al., JHMT 2016



Echelle locale: $\sim 100 \mu\text{m}$



$$\rho_{Nv} = \left| \frac{\sqrt{\tilde{\epsilon}_{veff}} - 1}{\sqrt{\tilde{\epsilon}_{veff}} + 1} \right|^2$$

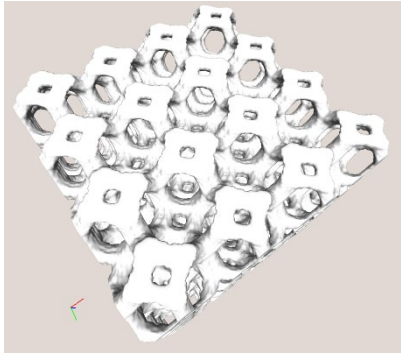


% énergie absorbée en fonction de
l'épaisseur de l'échantillon

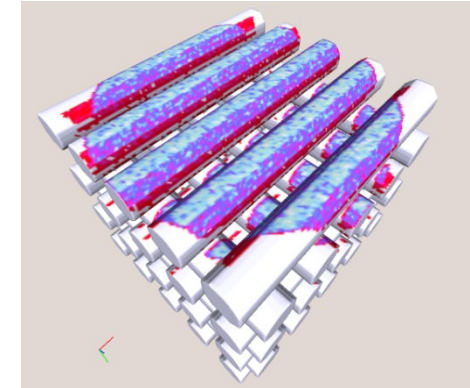
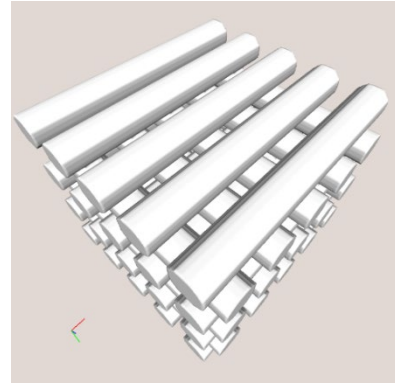
Comparaison céramiques poreuses cellulaires / céramiques poreuses régulières

$\rho \sim 80 \%$, $d_{\text{pore}} \sim 300 \mu\text{m}$, épaisseur = 2.5 mm

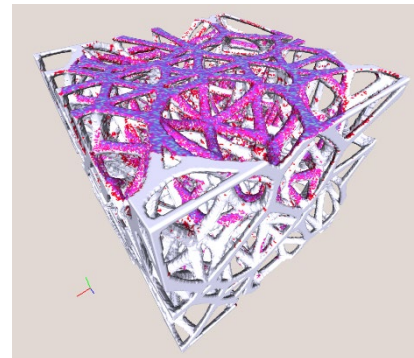
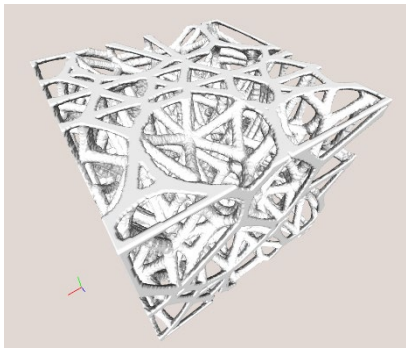
Cellule de Kelvin



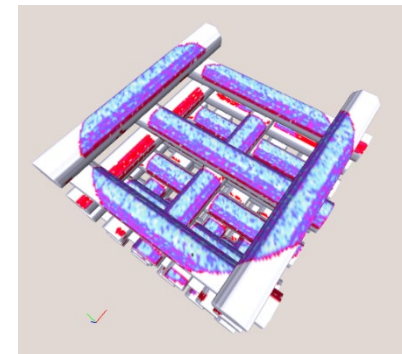
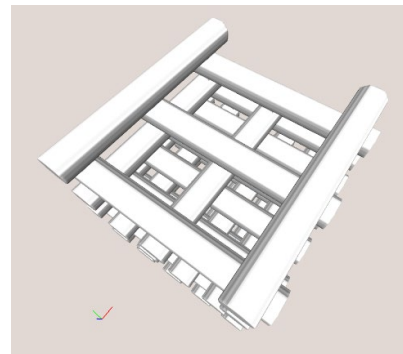
Structure régulière



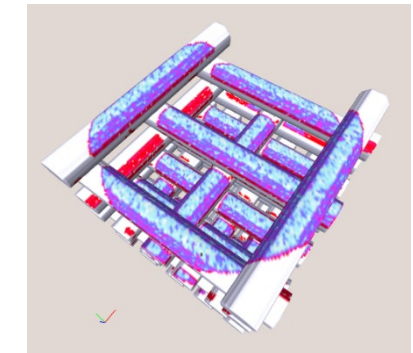
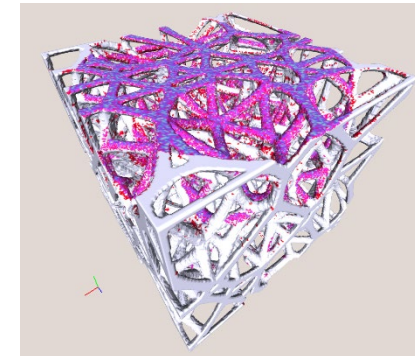
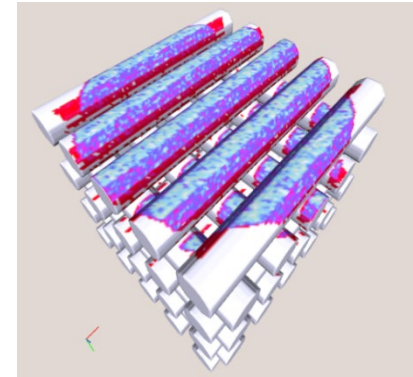
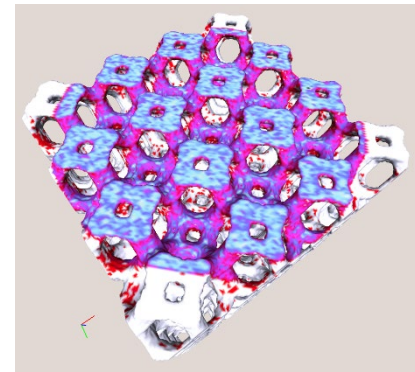
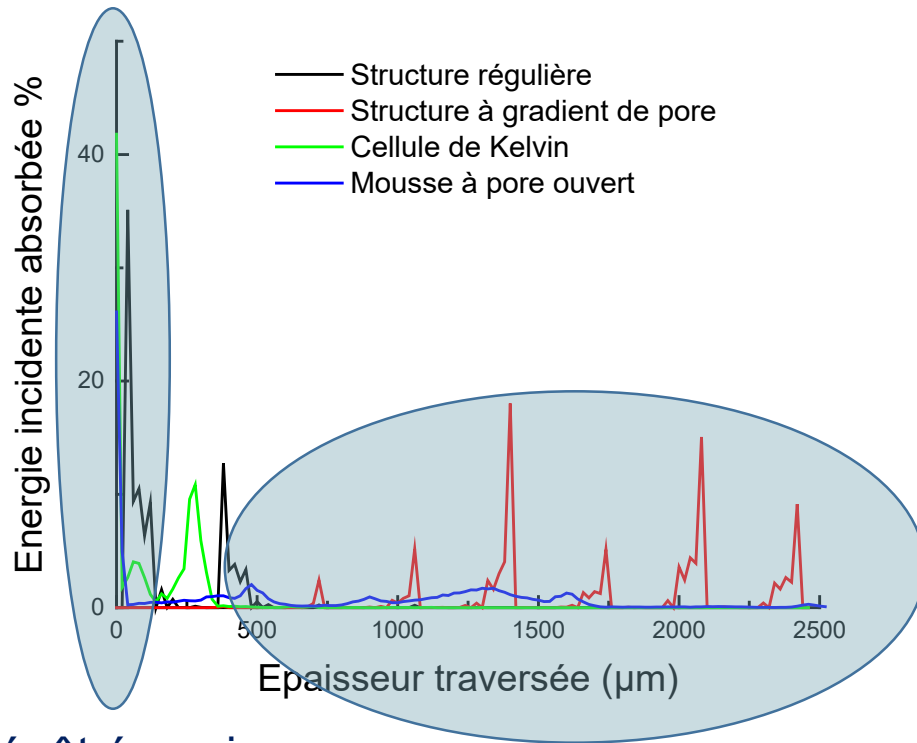
Mousse à pore ouvert



Structure à gradient de porosité



Absorption volumique du rayonnement



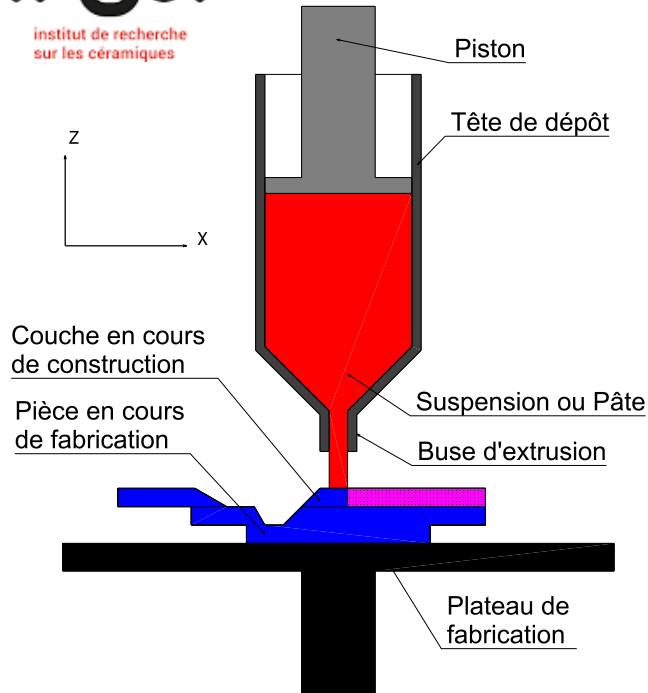
Dépôt énergie
pseudo-surface

Dépôt énergie en volume

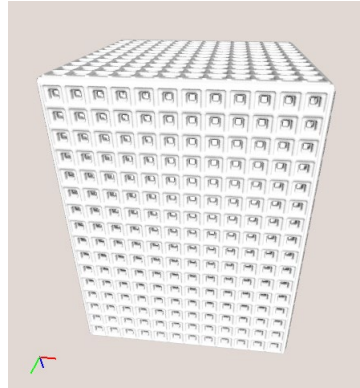
Elaboration de céramiques poreuses de CeO₂ par micro-extrusion

irCer

institut de recherche
sur les céramiques

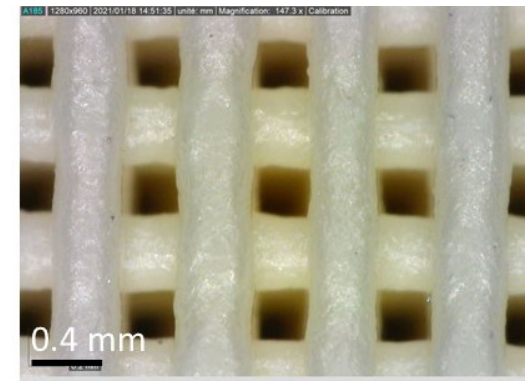
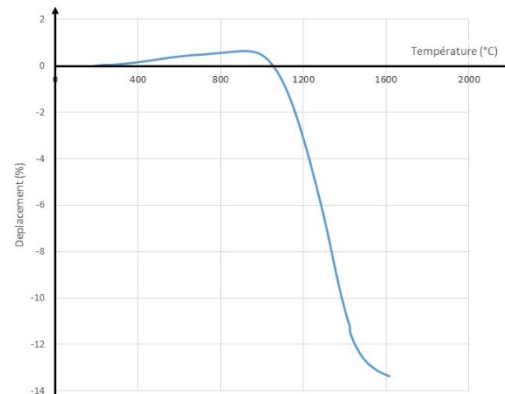
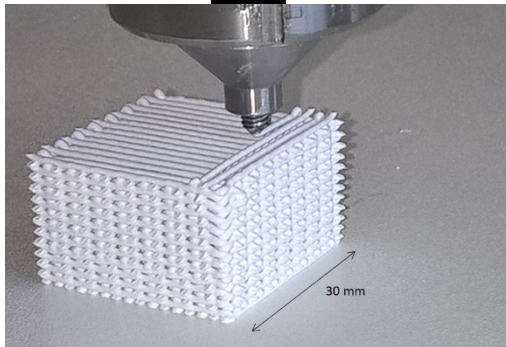
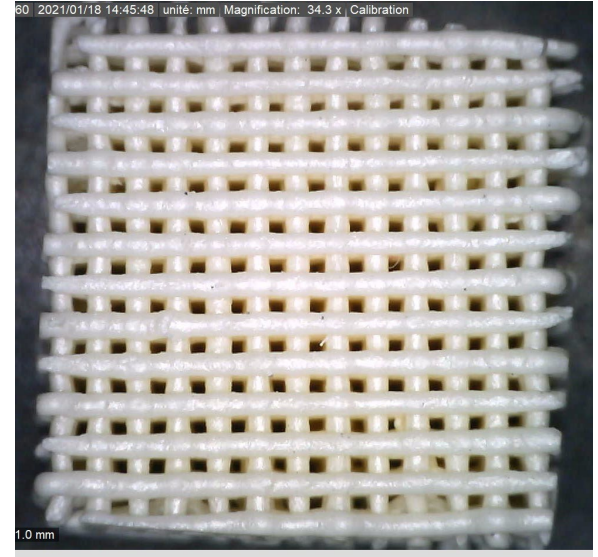


Maillage stl

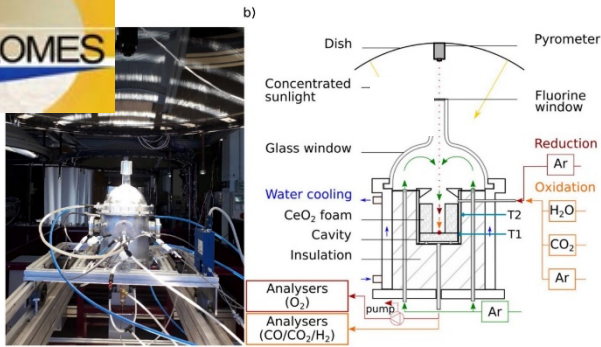


robocasting

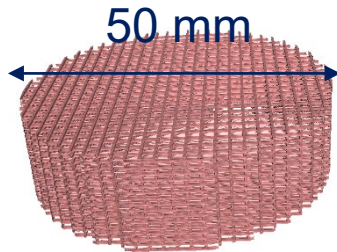
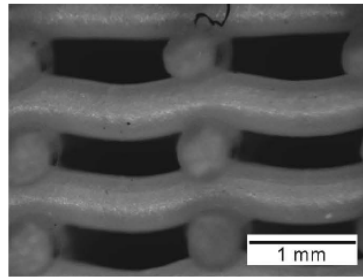
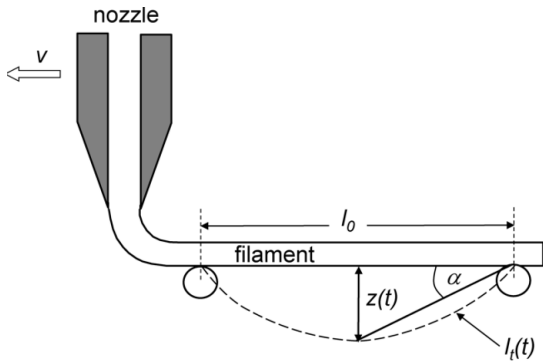
10 mm



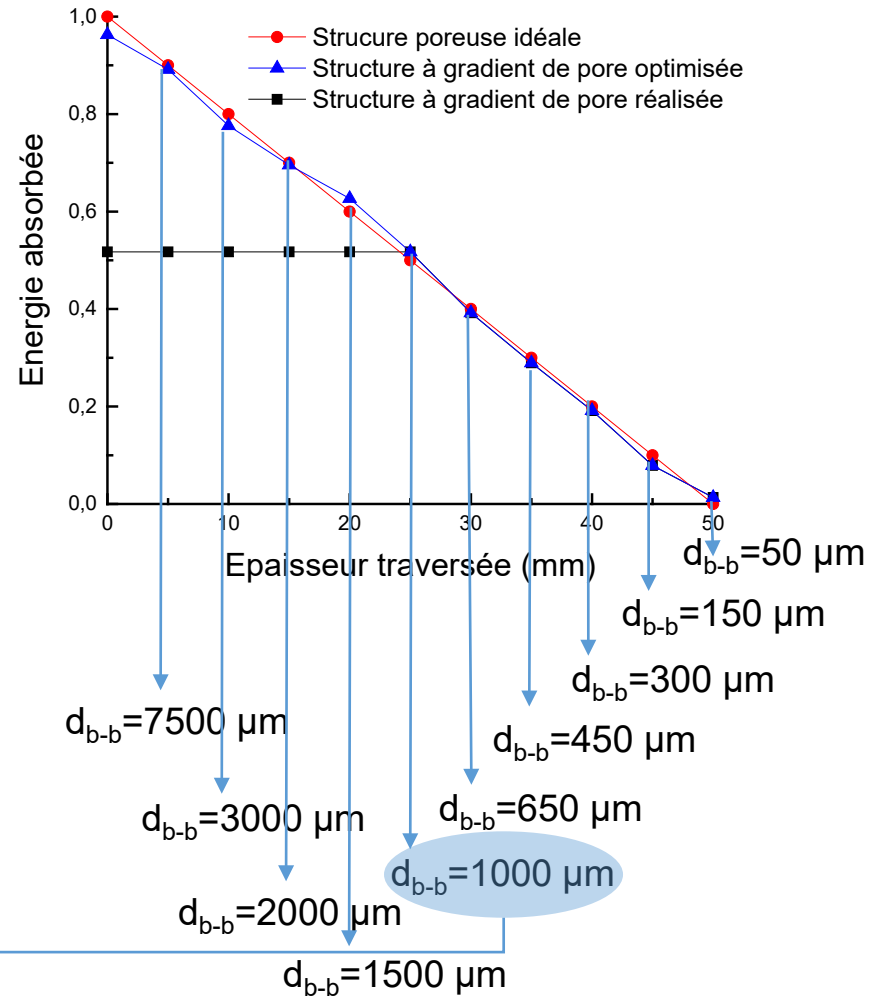
Conception numérique d'une céramique poreuse à gradient de porosité



Empilement de 10 blocs poreux à porosité descendante ($\varnothing = 50$ mm, épaisseur = 5 mm)

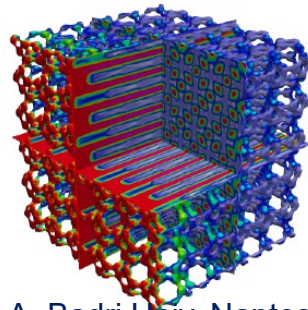


$d_b = 380 \mu\text{m}$



Conclusion et perspectives

- Production d'H₂ vert par thermochimie solaire
- Description statistique de la propagation volumique du rayonnement
- Optimisation de l'absorption volumique du rayonnement solaire → structures de CeO₂ à gradient de porosité
- Design radiatif numérique ↔ procédé de mise en forme ↔ génie des réacteurs solaires : structure poreuse à gradient de porosité
- Tests en réacteur réel au PROMES
- Calcul du champ de température par la méthode des éléments finis (FreeFem++, Y. Favennec, OPTHOCERA NExt) : problème thermo-fluidique avec pris en compte du rayonnement thermique
- Optimisation géométrique des céramiques de CeO₂ en tenant compte des transferts thermiques couplés



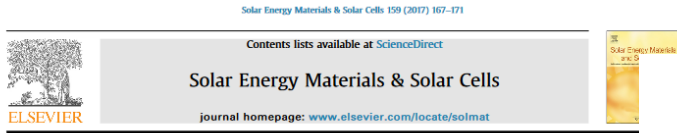
Th. A. Badri Univ. Nantes, 2018



celluleenergie.cnrs.fr

Programme 2020-2021 ThermASol :
LTen-IRCER-PROMES

Normal spectral reflectivity of $\text{CeO}_{2-\delta}$ ceramics



Spectral hemispherical reflectivity of nonstoichiometric cerium dioxide

Simon Ackermann, Aldo Steinfeld*

Department of Mechanical and Process Engineering, ETH Zürich, Sonneggstrasse 3, 8092 Zürich, Switzerland

ARTICLE INFO

Article history:
Received 23 August 2016
Accepted 31 August 2016
Available online 19 September 2016

Keywords:
Cerium
Nonstoichiometry
Reflectivity
Spectroscopy
Solar radiation

ABSTRACT

Nonstoichiometric ceria, $\text{CeO}_{2-\delta}$, has emerged as a promising redox material for thermochemical splitting of H_2O and CO_2 using concentrated solar energy. Knowledge of its radiative properties is crucial for the design of efficient solar reactors. Samples of various nonstoichiometries ($0 \leq \delta \leq 0.0377$) were prepared by thermal reduction in a thermogravimetric analyzer at high temperatures ($T > 1473 \text{ K}$) and low oxygen partial pressures ($p_{\text{O}_2} \leq 2.5 \cdot 10^{-4} \text{ atm}$). The spectral hemispherical reflectivity was measured using a spectroscopic goniometry system in the spectral range 300–2800 nm. A porous ceria with interconnected μm -sized pores showed comparable selectivity because of its high optical thickness. The spectral hemispherical reflectivity was computed for emission temperatures in the range 500–600 K relevant to solar reactors.

© 2016 The Authors. Published by Elsevier B.V. This is an open access article under the CC BY license (<http://creativecommons.org/licenses/by/4.0/>).



Checked with PROMES: $0 < \delta < 0.03$

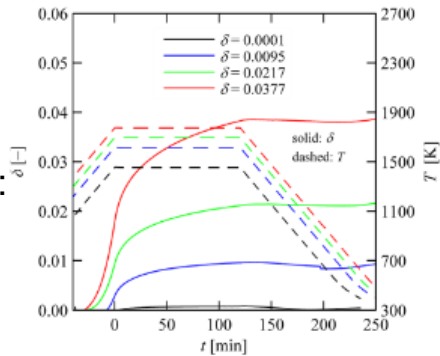


Fig. 2. Nonstoichiometry (solid) and temperature (dashed) of ceria as a function of time during a TGA run.

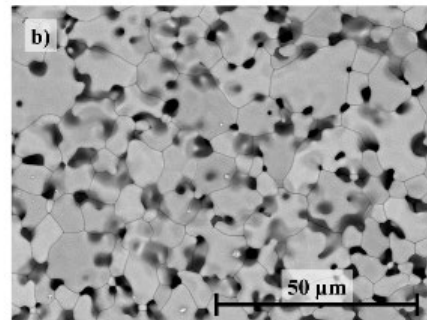
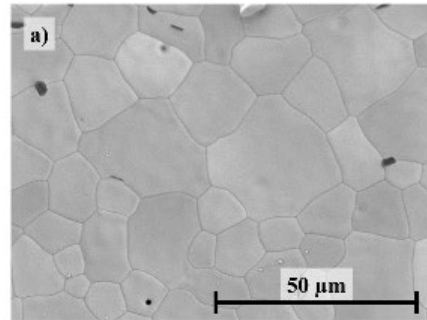


Fig. 3. SEM of the ceria pellets: a) non-porous; and b) porous with 0.26 porosity and 10 μm mean pore diameter.

Fig. 3. SEM of the ceria pellets: a) non-porous; and b) porous with 0.26 porosity and 10 μm mean pore diameter.

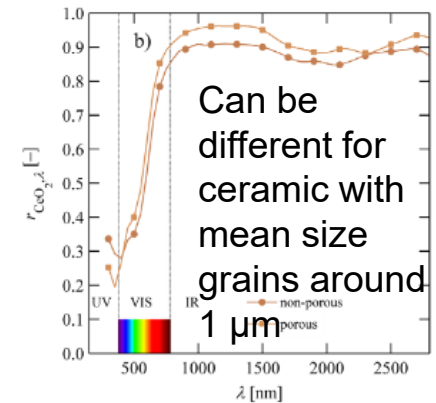
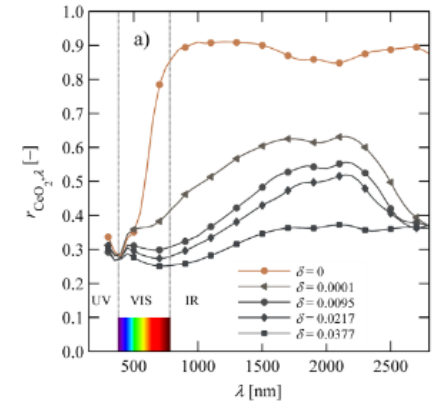


Fig. 5. Spectral hemispherical reflectivity of sintered polycrystalline ceria pellets as a function of the wavelength for: a) non-porous for various nonstoichiometries; and b) non-porous and porous for $\delta=0$. (For interpretation of the references to color in this figure, the reader is referred to the web version of this article.)

